Internal-state distribution of recombinative hydrogen desorption from Si(100)

Kurt W. Kolasinski,[a] Stacey F. Shane, and Richard N. Zare
Department of Chemistry, Stanford University, Stanford, California 94305

(Received 17 October 1991; accepted 27 November 1991)

We have measured vibrational- and rotational-state distributions for H_2, D_2, and HD thermally desorbed from the monohydride phase on Si(100) surfaces using resonance-enhanced multiphoton ionization detection. The $v = 1$ to $v = 0$ population ratio is roughly 20 times higher than that predicted by Boltzmann statistics at the surface temperature, $T_s \approx 780$ K. In contrast, the average rotational energies of the desorbed molecules are significantly lower than kT_s, exhibit no isotopic dependence within experimental error, and are not significantly different in the $v = 0$ and $v = 1$ vibrational states. In the vibrational ground state, we find $\langle E_{rot} \rangle = 345 \pm 83$ K, 451 ± 77 K, and 332 ± 57 K for H_2, HD, and D_2, respectively. The degree of vibrational excitation suggests that the H–H interatomic distance in the transition state is elongated compared with the gas-phase equilibrium bond distance. The low average rotational energy clearly rules out recombination from a highly asymmetric transition state or recombination from high-impact-parameter collisions. Our data may be interpreted as resulting from a preference for reactive trajectories that impart little angular momentum either through the effects of the corrugation of the potential-energy hypersurface or through the collision leading to the transition state, followed by prompt desorption of the newly formed molecular hydrogen from Si(100). We propose that pairing on Si dimers occurs prior to desorption; various models are discussed regarding the desorption mechanism subsequent to pairing.

I. INTRODUCTION

State-specific detection has been used extensively to probe scattering and thermal desorption at surfaces.[1] These studies have revealed much about the energy and momentum exchange processes that occur during gas–surface scattering and atomic and molecular desorption. Fewer state-specific studies have probed recombinative desorption from surfaces.[2-6] These studies, which have focused on desorption from the surfaces of metals, have used bulk permeation or chemical reactions to prepare the desorbing species.

A. Si(100)–(2×1) surface structure

Because a detailed knowledge of the geometric and electronic structure of Si(100)–(2×1) is important in the interpretation of our results, we present here a brief review of Si(100) surface physics. The Si(100) surface has been the subject of numerous investigations.[7,8] As with any well-studied system in surface science, the interpretation of experimental and theoretical investigations has not been without controversy. A growing consensus concerning the Si(100)–(2×1) surface is forming, however, largely arising from the insightful scanning tunneling microscopy (STM) work of Hamers, Tromp, and Demuth[9-12] and the convergence of theoretical work.[13-20]

The clean Si(100)–(2×1) surface exhibits a dimer reconstruction as depicted in Fig. 1. The driving force for the reconstruction is the elimination of the dangling bonds formed by truncation of the bulk structure. Dimer formation eliminates half of the dangling bonds by involving them in Si–Si bonds but leaves one dangling bond per Si dimer atom. This picture, however, has been found to be an oversimplification.

A controversy over the dimer structure, that is, whether the dimers are symmetric[13] or buckled,[21] has persisted for more than a decade. Hamers and co-workers,[10] using STM, have shown that symmetric dimers populate defect-free areas of the surface, whereas buckled dimers are found near vacancy defects. They have also shown that dimers persist to

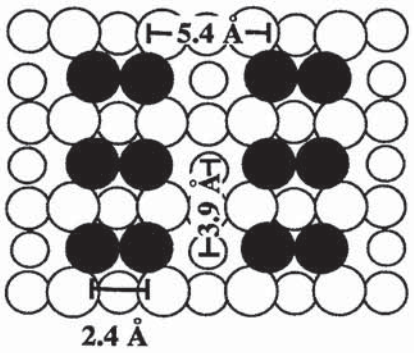

FIG. 1. A hard-sphere representation of the Si(100)–(2×1) surface. The dimer atoms are represented by the solid circles. Interatomic spacing values are those given by Hamers, Tromp, and Demuth (Ref. 10).

[a] Present address: Fritz-Haber-Institut der Max-Planck-Gesellschaft, Faradayweg 4-6, D-1000 Berlin 33, Germany.

 0021-9606/92/053995-12$06.00

the edges of, and even across, steps, and that although up to 10% of the surface is covered with vacancy defects, a very low density of Si atoms in the outermost layer exist singularly rather than in dimers. That both symmetric and buckled dimers are formed is not too surprising because calculations[16,17,20] have shown a small energy difference between the two structures. In fact, the true nature of the clean dimer may be that it is time-averaged symmetric, i.e., the dimer seesaws between two buckled configurations in such a way that it is on average symmetric at room temperature.[10,20]

The simple picture of an independent dangling bond existing on each dimer is also an oversimplification. Early calculations by Appelbaum, Baraff, and Hamann[13] indicated that these dangling bonds participate in a π-bonding interaction. This interaction is weak in that the bonding between the dimer atoms is not a true double bond. Appelbaum, Baraff, and Hamann estimated that the second "bond" is less than 40% of the strength of a Si–Si single bond, approximately 0.9 eV; recent calculations[22] set limits on a π-bonding interaction of 0.22–0.52 eV. A π-bonding stabilization has been confirmed by the scanning tunneling spectroscopy (STS) work of Boland[23] in which he estimates a stabilization of 0.8 eV. Other calculations[14,19] have shown that correlation between the electrons in the dimer bond is strong enough to induce antiferromagnetic ordering, i.e., a singlet ground state in the dimer π bond. This interaction makes the symmetric dimer the stabler configuration. Interactions between adjacent dimers are weak, however, with nearest-neighbor interactions on the order of 0.02 eV.[20]

Charge-density profiles[13,15,16] show that a better description of the state is a delocalized one that extends between both dimer atoms, although electron density from the highest-energy dangling-bond state is greatest immediately above the Si dimer atoms. This description is corroborated by the STM work of Hamers, Tromp, and Demuth[10] who found that a dimer appears as a beanlike shape; that is, the charge density of the occupied states above the dimer is delocalized over the dimer unit rather than appearing as two distinct dangling bonds.

The most important conclusion to draw from the electronic structure of Si(100) is that one independent dangling bond on each dimer atom represents an unstable configuration. The two electrons in the dangling bonds are correlated, not independent, and the dimer makes use of the correlation of these electrons to minimize its energy whether by π-bonding interaction, antiferromagnetic ordering, Jahn–Teller or Peierls distortion, or some combination of these.

B. Silicon hydride surface chemistry

The chemisorption of atomic hydrogen and desorption of molecular hydrogen on silicon surfaces has been studied extensively using numerous surface-science techniques.[24–29] For Si(100)–(2×1), adsorption of a single H atom onto a Si dimer breaks the π-bonding interaction of the dangling bonds and leads to a lone dangling bond on the Si atom not involved in the Si–H bond.[23] Saturation of the monohydride phase, that is, adsorption of two H atoms per dimer, appears to stabilize the symmetric dimer and relieves some of the subsurface strain associated with the reconstruction.[18,30,31]

The chemisorption of *molecular* hydrogen is poorly understood. Published values of the sticking coefficient of molecular hydrogen range from $\sim 10^{-6}$ to $\sim 10^{-3}$.[32–34] There are reports that the sticking of molecular hydrogen on Si(111) or polycrystalline Si surfaces appears to saturate at coverages on the order of a few percent of a monolayer.[32,35] This behavior would implicate the effects of special defect structures in the sticking of molecular hydrogen into these low coverage sites. Clearly, further critical investigation of the sticking dynamics for the H_2/Si system is needed.

Recent work[29] has suggested that thermal desorption from the surface of a covalent solid proceeds through a mechanism that differs markedly from the mechanism of desorption from the surface of a metal. The necessity of considering new models to explain recombinative desorption arises from experiments[27,29] that have shown that desorption from the monohydride phase on the Si(100)–(2×1) surface follows a first-order rate law, whereas desorption from Si(111)–(7×7) follows a second-order rate law.[26] Another experiment found that desorption from Si(111)–(7×7) at low coverage is described by kinetics that are intermediate between first and second order.[36] First-order desorption of hydrogen has also been observed from diamond,[37] germanium,[38] and tellurium[39] surfaces.

Sinniah *et al.*[29] reported the desorption activation energy E_{des} and Arrhenius prefactor A to be $E_{des} = 45 \pm 2$ kcal mol^{-1} (1.95 ± 0.09 eV) and $A = (2.2 \pm 0.3) \times 10^{11}$ s^{-1} from isothermal laser-induced thermal-desorption (LITD) studies. Wise *et al.*[27] reported $E_{des} = 58 \pm 2$ kcal mol^{-1} (2.52 ± 0.09 eV) and $A = (5.5 \pm 0.5) \times 10^{15}$ s^{-1} from LITD and 66 ± 4 kcal mol^{-1} (2.87 ± 0.18 eV) and $A = 6.5 \times 10^{17}$ s^{-1} from conventional thermal desorption. The values of A reported by Wise *et al.* appear high considering the known low sticking coefficient of H_2 (Refs. 32–34) and absence of reports of strong repulsive interactions between monohydride units. (See Ref. 40 and references therein for a complete discussion on factors influencing the Arrhenius prefactor.) The value reported by Sinniah *et al.* is consistent with the low sticking coefficient and suggests a constrained geometry in the transition state for desorption.

A first-order rate law is inconsistent with conventional hopping models[41] that appear to describe accurately the recombinative desorption of hydrogen from the surfaces of metals. Sinniah *et al.*[29] have proposed a model for desorption from the (100) surface in which the irreversible excitation of one hydrogen atom into a freely translating state precedes recombination of this atom with a normally bound atom. Wise *et al.*[27] have suggested a pairing model in which recombination occurs across a Si–Si dimer pair. Reider, Höfer, and Heinz[36] have proposed that a more conventional diffusion-based model, which incorporates recombination via at least two distinguishable sites, is active at low coverage on Si(111)–(7×7). Whatever the desorption mechanism, any model for the H/Si system must explain not only why recombinative desorption on semiconductors differs from that on metals but also why the desorption kinetics are structure sensitive for Si surfaces.

The formation of mono-, di-, and tri-hydride silicon spe-

cies follows the adsorption of either disilane, Si_2H_6 (as is used in our experiments; see below), or atomic hydrogen. Although the source of adsorbed hydrogen has little effect upon the properties of these hydrides,[28,42,43] the stability of the three surface hydrides depends on temperature and coverage. We typically use a crystal temperature of approximately 400 K during absorption. Such an elevated temperature suppresses the formation of higher hydrides and ensures that the Si surface is predominantly covered with the monohydride.[44] We note that at saturation coverage all of the surface dangling bonds are capped with adsorbed hydrogen, $H_{(a)}$.[43,45] Therefore, if we assume complete dissociation of Si_2H_6, one-third of the surface is covered with newly deposited Si, and the ratio of $H_{(a)}$ on "original" sites to $H_{(a)}$ on newly deposited Si is 2:1.

Under our experimental conditions, disilane adsorption and subsequent H_2 desorption result in the epitaxial growth of silicon. The surface is in the (2×1) reconstruction at the start and end of an experiment, but the surface structure at the time of H_2 desorption is not explicitly known. Recent STM work, however, has shown that ordered, monohydride-capped Si(100)–(2×1) surfaces result after briefly annealing Si_2H_6-saturated Si(100)–(2×1) surfaces to 670 K.[46] This temperature is roughly 100 degrees below the monohydride desorption temperature. Therefore, because of the reordering of the monohydride-covered surface[46] and the tendency of the Si(100) surface to form dimers even in the presence of defects,[10] we believe the majority of the adsorption sites should correspond to the dimer reconstruction, although the surfaces we use in this study may have some degree of disorder and H atoms adsorbed in sites other than ideal Si dimer units. Furthermore, we have found[47] that internal-state distributions are insensitive to whether the source of adsorbed hydrogen is Si_2H_6 or atomic H.

Below, we present data on the rotational- and vibrational-state distributions of H_2, HD, and D_2. Our results indicate that the mechanism of recombinative desorption of molecular hydrogen from Si(100) leads to rotational distributions colder than the surface temperature; we conclude that little torque is applied to the molecule during the recombinative process. An accurate model of recombination must include a dynamical constraint that causes an exaggerated population of low rotational states. The vibrational distributions reveal that more energy is deposited in the vibrational degree of freedom than would be expected from Boltzmann statistics at the surface temperature. Our results can be made consistent with the delocalized band-state model[29] by involving some sort of constrained diffusion, that is, a model in which diffusion proceeds only along certain crystallographic directions. However, we assert that a pairing model is in much better accord not only with our data, but also with dynamical models of recombinative desorption and with the electronic and geometric structure of Si(100)–(2×1).

II. EXPERIMENT

Internal-state distributions of molecular hydrogen are determined using a $(2+1)$ resonance-enhanced multiphoton ionization (REMPI) scheme utilizing the $E, F\,^1\Sigma_g^+$ state as an intermediate state.[48] This scheme requires ultraviolet radiation in the wavelength range of 200–215 nm to probe $v=0$ and 1. This light is generated by a Nd:YAG-pumped dye laser. Blue-shifted rhodamine 640 (shifted by addition of a few drops of a NaOH dissolved in methanol) or a mixture of DCM and rhodamine 610 dyes dissolved in methanol is used in the dye laser. The dye laser output is first frequency doubled in a potassium dihydrogen phosphate (KDP) crystal. The doubled light is then frequency mixed with residual dye laser fundamental in a β-barium borate (BBO) crystal.[49] This procedure routinely produces 1–2 mJ of light in the wavelength region of interest, sufficient to completely saturate the $(2+1)$ process. Unwanted frequency components are separated from the tripled light by the use of dichroic mirrors, which also serve to define the optical path into the ultrahigh vacuum (UHV) chamber. The laser beam propagates parallel to the Si(100) crystal face and is focused a few millimeters above the surface using a 350 mm lens. The detection region of the experimental apparatus is depicted schematically in Fig. 2.

Ions produced in the REMPI process are extracted into a mu-metal-shielded time-of-flight (TOF) tube in which they are counted using a chevron (two-stage multichannel plate) detector. The output of the chevron detector is collected by a gated integrator and stored by a minicomputer for subsequent analysis. The ion signal is normalized on a shot-by-shot basis to the output of a pyroelectric detector that monitors the power of the tripled light. This method of

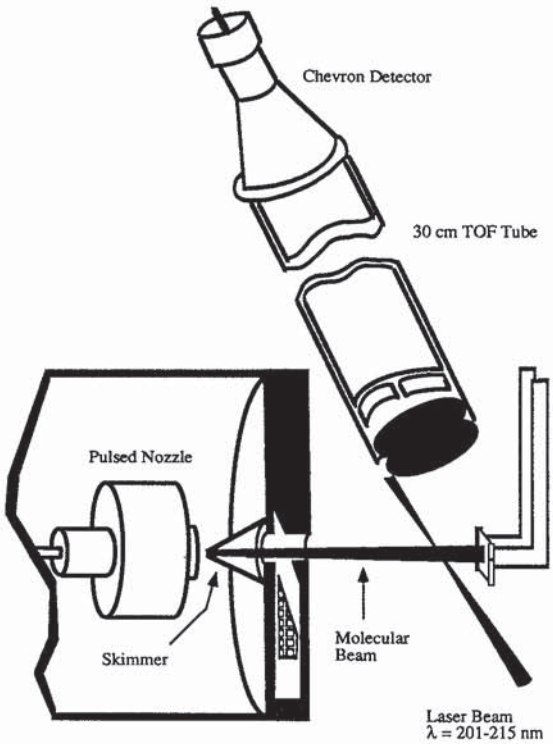

FIG. 2. Schematic drawing of the detection region of the experimental apparatus.

state-specific detection has a sensitivity on the order of 5×10^5 molecules per quantum state per cm.[3] We have calculated that even for unrealistically large velocity differences between H_2 and D_2, our data will be affected to a degree much less than our one σ error bars by corrections for changes in detection efficiency with velocity or by corrections in comparing ion signals to desorption fluxes.

The UHV chamber is evacuated by a turbomolecular pump to a base pressure of approximately 2×10^{-10} Torr. Surface order and cleanliness are checked with low-energy electron diffraction (LEED) and Auger electron spectroscopy (AES). The 10×13 mm rectangular Si(100) crystals are highly As doped (0.005 Ω cm) to facilitate direct resistive heating under computer control. The computer generates a set point for an external feedback circuit. The set point is updated at 10 Hz with a rate of change determined by the computer. The feedback circuit, not the computer, directly monitors the crystal temperature via Chromel–Alumel thermocouples affixed to the Si with either alumina- or zirconia-based adhesives. The crystal and manipulator are liquid-nitrogen cooled.

Sample preparation consists of degreasing the Si(100)–(2×1) wafers with successive ultrasonic baths of methanol, acetone, and ethanol. Most of the samples were not etched prior to insertion into the vacuum chamber. Some were etched in NH_4F or HF solutions and rinsed in distilled water and ethanol. No correlations were observed between sample pretreatment and internal-state distributions. During the last 12–24 h of bakeout the crystal is held just below the desorption temperature of the native oxide to thoroughly degas the manipulator and Nb crystal holder before exposing the bare Si surface. After the chamber cools down, the oxide is desorbed by annealing the crystal at 1200 K. The crystal is then cooled at 1–2 K s^{-1}. This procedure yields a well-ordered Si(100)–(2×1) surface that generally has some residual carbon contamination.

At the end of each day we passivated the crystal with a large dose of disilane. At the beginning of each day, the passivating layer of $H_{(a)}$ was desorbed and the crystal annealed at 1000 K for 10–15 min, then cooled at 1–2 K s^{-1}. High-temperature annealing was avoided to lessen the likelihood of surface roughening. This procedure led to a gradually increasing level of C contamination over the period of weeks. No correlation between C coverage and internal-state distributions was found. Crystals were used as long as the LEED pattern remained sharp. A total of 12 different crystals were used during this study. No correlations between crystals and internal-state distributions were found. Data from one crystal was disregarded because of a second lower-temperature hydrogen desorption feature of uncertain origin. The main desorption feature from this surface, however, yielded rotational distributions consistent with the results of the other crystals.

Experiments are performed by dosing the Si(100)–(2×1) surface to saturation using a pulsed, skimmed, and collimated molecular beam of disilane. The nozzle delivers pulses at 10 Hz with a temporal width of approximately 2 *ms*. The molecular beam strikes the surface at normal incidence. A sufficient stagnation pressure of disilane is used, typically 30–60 Torr, to saturate the surface in 30–60 s.

We used a molecular beam of disilane as a source of adsorbed hydrogen because of several practical advantages. The sticking coefficient of disilane is on the order of 10^{-1}, higher than that of H_2 or SiH_4 by 4 to 5 orders of magnitude.[50,51] Consequently, we can avoid extreme exposure conditions, i.e., high pressures and long durations, that could lead to contamination of the surface.[52] A hot filament source of more reactive, vibrationally excited hydrogen and atomic hydrogen, commonly used for dosing hydrogen, also requires high exposures, may lead to surface etching, and doses all exposed surfaces. A molecular beam represents a relatively simple and reliable system that will dose only a small portion of the crystal. This system allows us to avoid spurious signals caused by desorption from surfaces other than Si(100) and minimizes the effects of temperature inhomogeneities across the crystal face by virtue of the molecular beam's small spot size (approximately 4 mm in diameter). A heated-nozzle molecular beam source of hydrogen would have similar advantages but could not be easily adapted to our experimental chamber.

After dosing the crystal, we perform a temperature-programmed desorption (TPD). We use the REMPI/TOF scheme to collect the desorption spectrum one rovibrational quantum state at a time. In this procedure, the laser is tuned to a transition corresponding to a specific (v,J) level. Ions created in the REMPI process are then collected as a function of crystal temperature. The heating rate is 10 K s^{-1} and 20 laser shots are averaged into one bin. Because our laser operates at 10 Hz, the ion signal is collected in bins that span 20 K in surface temperature. The maximum in the thermal desorption flux occurs in the range 780–800 K. During data acquisition the computer controls the heating rate but does not directly monitor the crystal temperature, and our desorption spectra are taken vs time. The desorption temperature we quote here is based on the work of Sinniah *et al.*[29] and is consistent with our own less accurate measurements. At the end of each desorption run, the crystal is annealed from one half to several minutes before being cooled at 3 K s^{-1} to assure reordering of the surface and epitaxial growth of Si. In general, this procedure is repeated 3–5 times before proceeding to the next J level.

The $(2+1)$ REMPI process through the $E,F\,^1\Sigma_g^+$ state is well characterized.[48] Specifically, ionization probabilities for H_2, HD, and D_2 are known for all of the (v,J) levels used in this work. Little variation in ionization probability with J is apparent, although the relative ionization probability does change significantly with v.

We have compared two methods of reducing signal strengths to rotational populations: full peak integration and peak-height analysis. Full peak integration corresponds to an average over the entire accessible coverage range (0–1.0 ML of $H_{(a)}$ relative to Si; ML denotes monolayer) and a surface temperature range of $\Delta T_s = 60$–80 K. Peak-height analysis corresponds to the signal from a smaller coverage range centered about half the saturation coverage and a surface temperature range of 20 K. Both methods yield the same rotational distributions within error bars. The results we present were obtained using full-peak integration.

III. RESULTS

A. Rotational distributions

Using the experimental method outlined above, we have obtained data for the thermal desorption from Si(100) of H_2 (by dosing Si_2H_6), D_2 (dosing Si_2D_6), and HD (dosing a mixture of Si_2H_6 and Si_2D_6). Figure 3 shows a typical thermal desorption spectrum of $H_2(v=0, J=1)$. This raw data must be corrected for two distinct background contributions: (1) ambient hydrogen present in the vacuum chamber, and (2) hydrogen that has thermally desorbed from the Si(100) surface and entered the laser focal volume *after having undergone a number of collisions with the chamber walls.*

The former type of background signal is constant over a desorption spectrum and is easily accounted for by simply setting the base line for integration at an appropriate offset. The second type of background signal requires a more involved subtraction technique in which independent experiments are performed to determine the temperature of the background gas and the fraction of the signal caused by the background.

The temperature of the background hydrogen is determined by dosing the crystal in the usual fashion. The laser, however, is placed vertically above and slightly behind the crystal face. In this way the focal volume does not intercept any of the directly desorbed hydrogen. Using this experimental geometry, we have determined that background hydrogen is equilibrated with the chamber walls (300 K).

This experiment cannot be used to determine the percentage of signal arising from background gas because the detection efficiency depends sensitively on the detection geometry. By moving the laser above the crystal, our detection sensitivity decreases by at least a factor of 2 to 4. Furthermore, the percentage of nascent signal to background signal is a function of the location of the focal volume relative to the surface because of the different angular distributions of the two types of signal [$(\cos\theta)^n$ vs isotropic].

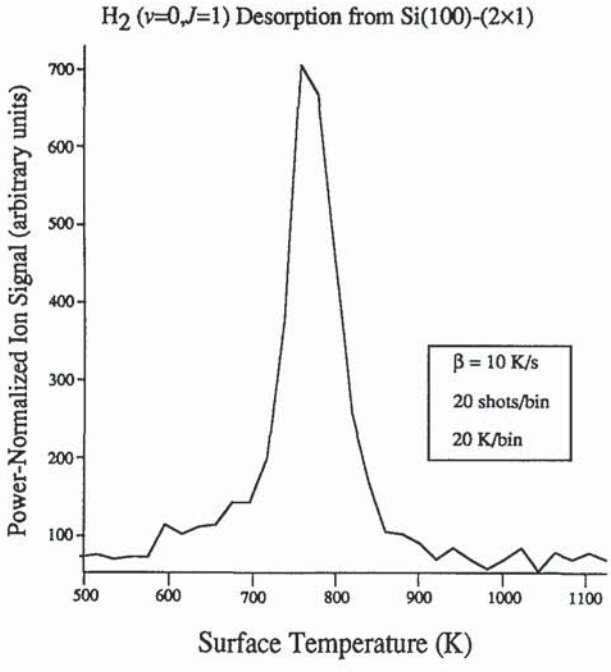

FIG. 3. Thermal desorption spectrum for $H_2(v=0, J=1)$ desorbing from Si(100)-(2×1) after a saturation dose of Si_2H_6. The surface temperature during adsorption is approximately 400 K.

To determine the percentage of our signal arising from background gas, we backfill the chamber to a known pressure of hydrogen, typically about 1×10^{-9} Torr, after dosing the crystal in the usual way with the normal detection geometry. We then perform a TPD in the usual manner and measure the pressure rise in the system, the base-line ion signal level (i.e., the ion signal of the backfilled hydrogen), and the desorption ion signal. The known pressure of backfilled hydrogen allows us to calibrate the ion signal we observe so that we can convert counts of signal into effective pressure units. The ion signal from the desorption peak can then be converted into an effective pressure. This value is the effective pressure of nascent hydrogen plus background hydrogen. The pressure of the background hydrogen that reenters the focal volume after relaxation is equal to the transient pressure rise measured in the chamber. By repetitively performing this experiment, we have determined that nascent hydrogen constitutes $70\pm5\%$ of our signal from either $H_2(v=0, J=1)$ or $D_2(v=0, J=2)$ i.e., $30\pm5\%$ of our signal is from collisionally relaxed hydrogen. Because we also know the temperature of the background gas, we can accurately subtract the appropriate amount of background signal from the signal for each (v, J) transition.

Cursory attempts to detect any background in $v=1$ have been unsuccessful as was also observed by Kubiak, Sitz, and Zare for H/Cu.[2] This result is not surprising, as vibrational deactivation in the collisions of gases with rough surfaces has been shown to be very efficient even when the gas–surface attractive interaction is weak.[53–55] Therefore, we assume there is no background contribution to the $v=1$ data.

Figure 4 displays a Boltzmann analysis of the rotational populations for H_2, HD, and D_2 in the first two vibrational states after background subtraction. Here, we have plotted vs rotational energy the natural logarithm of the power-normalized ion signal divided by the rotational-state degeneracy $(2J+1)$, the nuclear-spin degeneracy (g_N), and the appropriate v-, J-, and isotopomer-dependent correction factor.[48] The data for H_2 accurately represent the $v=0$ to $v=1$ population ratio. The curves for HD and D_2 have been offset by constant factors to emphasize the similarity in shapes for the rotational distributions. Should such a plot yield a linear relation, the slope of the line is related to a "temperature" and indicates that the system follows Boltzmann statistics.

The large rotational constant of molecular hydrogen combined with low rotational excitation means that few rotational levels are significantly populated. Signal from rotational levels higher than those shown in Fig. 4 has been acquired on occasion but has been deemed too uncertain to include in our analysis. The paucity of accessible rotational levels makes it difficult to discern trends in the distribution as a function of J and can make a Boltzmann analysis misleading. Therefore, we prefer to characterize the distributions using a vibrational-state-dependent average rotational

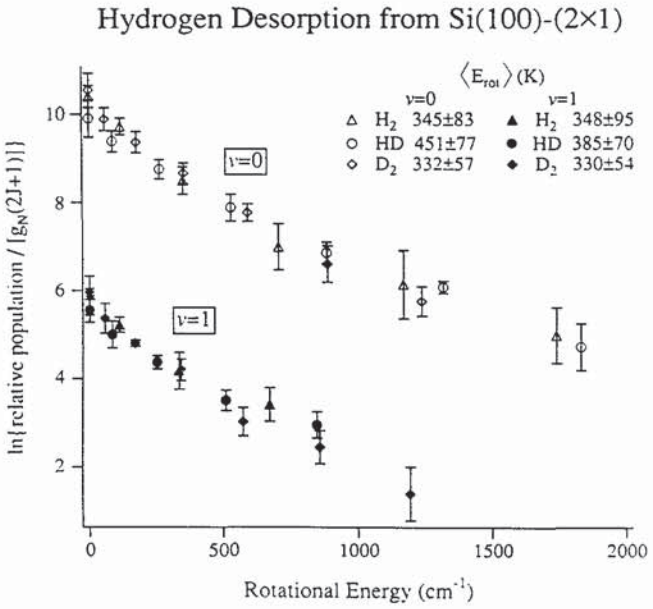

FIG. 4. Boltzmann plot of H_2, HD, and D_2, thermally desorbed from Si(100)-(2×1). The data has been corrected for background contributions as explained in the text. $T_s \approx 780$–800 K. Rotational distributions are comprised of J levels 0–5, 0–6, and 0–6 for $v = 0$ of H_2, HD, and D_2, respectively, and 0–3, 0–4, and 0–6 for $v = 1$ of H_2, HD, and D_2, respectively.

energy, $\langle E_{\rm rot}\rangle(v)$, rather than a rotational temperature. For this purpose we use the relation

$$\langle E_{\rm rot}\rangle(v) = \Sigma_J N_{vJ} E_J / \Sigma_J N_{vJ},$$

where N_{vJ} is the population of the rotational state J in arbitrary units and E_J is the rotational energy of that state. The observed values of $\langle E_{\rm rot}\rangle(v=0)$ are 345 ± 83 K, 451 ± 77 K, and 332 ± 57 K for H_2, HD, and D_2, respectively, and of $\langle E_{\rm rot}\rangle(v=1)$ are 348 ± 95 K, 385 ± 70 K, and 330 ± 54 K for H_2, HD, and D_2, respectively. Complete rotational distributions were collected 10–16 times each for H_2, HD, and D_2 in $v = 0$ and 4, 1, and 5 times for H_2, HD, and D_2, respectively, in $v = 1$. Therefore, the error bar for HD ($v = 1$) is an indication of the single experimental uncertainty without any contribution from the variability of results from experiment to experiment. The latter accounts for the uncertainty in the other reported values. Note that (1) all three isotopomers exhibit significant rotational cooling in desorption (compared to $T_s \approx 780$ K), (2) the rotational distributions do not vary significantly between the $v = 0$ and $v = 1$ states, (3) $\langle E_{\rm rot}\rangle$ is essentially the same for all three isotopomers, (4) deviations from Boltzmann statistics are manifested by curvature in the Boltzmann plots, and (5) ortho and para states of H_2 and D_2 are populated statistically.

B. Vibrational distributions

Once the rotational distributions of the $v = 0$ and $v = 1$ states have been determined, we may determine the population ratio between these two vibrational states. We sum the populations of the J levels for the two vibrational states to determine this ratio. The dependence of the relative ionization probabilities on vibrational states is known;[48] however, to compare data from different experimental runs accurately, we collect signal for transitions in the two vibrational states during several experimental runs. In general, we obtain this ratio by first measuring the signal for one (v,J) transition, for example, $H_2(v = 1, J = 1)$. We then obtain a complete rotational distribution from the other vibrational state; the first measured transition is the corresponding J level of the other vibrational state, $H_2(v = 0, J = 1)$ in this example. In this manner we can record data for the population ratio with the most consistent possible experimental conditions. This ratio was measured 5, 7, and 7 times for H_2, HD, and D_2, respectively. Attempts to detect signal from the $v = 2$ state were unsuccessful.

Table I displays the data pertinent to the vibrational population analysis for the three isotopomers. We find the experimentally determined $v = 1$ to $v = 0$ population ratio, $R_{\rm expt}$ to be $R_{\rm expt}(H_2) = 0.0116 \pm 0.005$, $R_{\rm expt}({\rm HD}) = 0.021 \pm 0.015$, and $R_{\rm expt}(D_2) = 0.081 \pm 0.040$. Because we have found no background in the $v = 1$ level, we have not subtracted a background contribution from the $v = 1$ data. We can calculate the vibrational population ratio expected for a Boltzmann distribution at the surface temperature (we choose T_s at the desorption peak maximum, $T_s = 780$ K) according to the equation

$$R_{\rm Boltz} = \exp(-\nu_{01}/kT_s),$$

where ν_{01} is the origin of the first vibrational state in $\rm cm^{-1}$,

TABLE I. The experimentally determined vibrational-state population ratios $R_{\rm expt}$ are presented for the three hydrogen isotopomers and compared with the ratios expected from Boltzmann statistics, $R_{\rm Boltz}$, at a surface temperature of 780 K. The ratio between these values, the energy spacing between vibrational states ν_{01} and the experimentally determined average rotational energies $\langle E_{\rm rot}\rangle$ are also listed.

	H_2	HD	D_2
ν_{01} ($\rm cm^{-1}$)	4164.14	3632.10	2993.98
$R_{\rm expt} = N_{v=1}/N_{v=0}$	0.0116 ± 0.005	0.021 ± 0.015	0.081 ± 0.040
$R_{\rm Boltz} = \exp(-\nu_{01}/kT_s)$	0.000 465	0.001 23	0.00400
$\langle E_{\rm rot}\rangle(v=0)$ (K)	345 ± 83	451 ± 77	332 ± 57
$\langle E_{\rm rot}\rangle(v=1)$ (K)	348 ± 95	385 ± 70	330 ± 54
$R_{\rm expt}/R_{\rm Boltz}$	25.0 ± 9.9	17 ± 12	20.1 ± 9.9

and k is the Boltzmann constant expressed in $cm^{-1}\ K^{-1}$. Note the values obtained from this equation in Table I. A comparison of the values of R_{Boltz} to those for R_{expt} shows that all three isotopomers exhibit enhanced population of the $v = 1$ level relative to Boltzmann statistics, and the enhancement factor is roughly equal in all three cases within error bars. Specifically, we find the ratio R_{expt}/R_{Boltz} to be 25.0 ± 9.9, 17 ± 12, and 20.1 ± 9.9 for H_2, HD, and D_2, respectively.

Correlation between velocity and vibrational state is expected if there is strong vibrational-to-translational coupling in desorption. In this case hydrogen in $v = 1$ will have a lower velocity than hydrogen in $v = 0$. Our detector is primarily a flux detector with some density contribution; therefore, we directly measure flux and our reported vibrational ratios do not need to be corrected for velocity. Rough calculations indicate that even if the mean translational energy of hydrogen in $v = 1$ is the equivalent of one vibrational quantum lower than the mean translational energy of hydrogen in $v = 0$, the data will be unaffected with regard to either the absolute value or isotopic trend of the vibrational enhancement factor.

IV. DISCUSSION

A. Vibrational distributions

We have determined that the population of the $v = 1$ state is roughly 20 times that expected for an equilibrium distribution at T_s. Superthermal vibrational population of $v = 1$ was observed in the recombinative desorption of hydrogen from Cu(111) and Cu(110),[2] as well as for the recombinative desorption of N_2 from S-covered poly-Fe.[3] Enhanced population of $v = 1$ has also been reported for the D_2/Pd(100) (Ref. 4) and D_2/S-covered poly-Pd (Ref. 56) systems, but to a smaller degree.

Relaxation of the vibrational degree of freedom for hydrogen is a slower process than is relaxation of rotation. As we will demonstrate below, exit channel effects are minimal in the consideration of the rotational distributions; thus, we can neglect them entirely in the analysis of the vibrational distributions. We conclude that the vibrational and rotational distributions we obtain are directly related to the recombinative event and unmodified by interactions along the exit channel.

The degree of vibrational excitation is indicative of the extent to which the desorption transition state resembles the gas-phase hydrogen molecule. A transition state in which the H–H bond distance is elongated compared with the equilibrium bond distance of molecular hydrogen in the gas phase, r_e, would result in vibrational excitation of the product H_2. This correlation has been confirmed for the H/Cu system in the calculation of Harris, Rahman, and Yang.[57]

No accurate potential-energy hypersurface exists for the H/Si(100) system. Our observation of vibrational excitation, coupled with gas-phase reaction propensity rules[58] and theoretical confirmation,[59,60] leads us to predict that the potential-energy hypersurface must have a central or late barrier to adsorption. That is, the saddlepoint in the interaction potential for $H_{2(g)} + Si(100) \rightarrow 2H_{(a)}/Si(100)$ is located at a somewhat extended H–H distance relative to r_e. This topography will lead to vibrational-to-translational energy transfer in adsorption as observed in the H/Cu system.[61–64] However, in comparison to the H/Cu system, *we observe a significantly lower vibration enhancement factor even though indications are that the barrier height is much higher in the H/Si system.*[65] Therefore, we believe that the H_2 molecule is not extensively stretched in the transition state.

The uniformity of vibrational enhancement factors demonstrates the importance of accurate quantum-mechanical calculations for complete interpretation of the data. Because of the small mass and large zero-point energy of H_2, the effects of tunneling must be considered. We believe, however, that tunneling is not important on the scale of our error bars in the desorption of hydrogen from Si(100) since each of the isotopomers exhibits the same vibrational enhancement factor relative to a Boltzmann distribution and, furthermore, the rotational distributions exhibit the same average rotational energy for all three isotopomers in both $v = 0$ and $v = 1$.

The basic physics of dissociative hydrogen adsorption within a jellium framework is illustrated in the calculations of Nørskov, Johansson, and co-workers.[66–68] The use of a jellium model to describe the H/Si system is obviously an oversimplification. Harris has elaborated upon the features of this model and its limitations.[69] An essential feature of dissociative H_2 adsorption (or, conversely, recombinative H_2 desorption) is the filling (emptying) of the hydrogen antibonding resonance. Since hydrogen is a closed-shell molecule, it essentially acts as a noble gas as it approaches the surface. After a weak van der Waals interaction, the hydrogen–surface potential becomes strongly repulsive. As the surface electrons interact with hydrogen, they broaden and lower the energy of the molecular antibonding state; eventually this level drops below the Fermi energy and becomes partially occupied. The hydrogen bonding level also broadens and shifts downward as it mixes with the electronic states of the surface, but to a lesser degree. During this process the H–H attraction decreases while the H–surface attraction increases.

The height of the activation barrier is sensitively dependent on the shapes of the H–H and H–surface potential curves and the position of their crossing point. The presence of d electrons can significantly lower this barrier.[70] Since the dangling-bond state of Si(100)–(2×1) is composed of sp^3 electrons and there are no nearby d-electron states, significant electronic rearrangement must occur to overcome the Pauli repulsion with the H_2 $1\sigma_g$ level (filled bonding orbital) and to allow the hydrogen-antibonding resonance to fill. Thus, we expect a substantial activation barrier. Distortion of the molecule through bond elongation will accompany and facilitate the filling of the antibonding resonance.

Although the hydrogen molecule is accurately treated in the model of Nørskov and co-workers,[66–68] an essential feature of the Si surface, namely the localized dangling-bond states, is poorly represented. The basic elements of this model, however, should be active in any hydrogen adsorption system that results in adsorbed hydrides. That is, in the final state an adsorbed H atom has an increased electron density

compared with an isolated H atom; therefore, a net donation of electrons to the H atom occurs. This is the case in the adsorption of H on Si.[18,71] The ramifications of the inaccuracies of the jellium treatment are discussed further with the rotational distributions. This model does, however, adequately treat the gross aspects of the essential dynamics involved, and it presents a solid conceptual framework.

We cannot determine the height of the activation barrier solely by determining the vibrational population. In fact, the height of the activation barrier to adsorption is purely a one-dimensional concept. The effective height of the barrier depends on the shape of the potential-energy hypersurface, the position of the barrier maximum, the orientation of the molecule, and the point of impact in the surface unit cell. To determine the barrier height the total energy of the desorbing particle and the partitioning of that energy must be measured.[60] With use of our experimental method the translational energy may be probed by determining the Doppler width of the spectral transitions if some assumption concerning the angular distribution of desorbing molecules is made. We have not yet performed such an experiment. Preliminary experiments performed elsewhere indicate that the translational energy required to overcome the barrier is substantial and that the barrier is probably greater than 1 eV.[65]

In observing superthermal vibrational excitation we must answer the question: What is the cause of this excitation? The recombination of two $H_{(a)}$ to form $H_{2(g)}$ results in the formation of one H–H bond worth 104 kcal mol^{-1} at the expense of breaking two Si–H bonds. The exact strength of the Si–H bond on a Si surface is disputed[27] but is roughly 80 kcal mol^{-1}. Therefore, the recombinative desorption of H_2 is roughly 60 kcal mol^{-1} *endo*thermic and, hence, the heat of reaction is not responsible for superthermal vibrational excitation.

The shape of the potential-energy hypersurface must therefore lead to vibrational excitation. An activation barrier, in a sense, acts as an energy dam, forcing energetic $H_{(a)}$ pairs to build up on the surface until they overflow the activation barrier. Since the top of the activation barrier is above the energy zero of the gas-phase H_2 molecule, a superthermal energy distribution of desorbed H_2 is possible as long as the desorbing molecule does not equilibrate with the surface during desorption. Acceleration during descent of the activation barrier inhibits surface accommodation while location of the barrier at an elongated H–H distance relative to r_e channels energy into the vibrational coordinate. We conclude that hydrogen molecules leave the surface promptly after recombination with little molecule–surface energy exchange and that, therefore, an activation barrier is responsible for the excess vibrational energy we observe.

B. Rotational distributions

As mentioned above, the adsorption of hydrogen onto Si(100) is activated. We cannot predict *a priori* how the energy required to surmount an activation barrier will be partitioned in the product molecule. This energy partitioning is determined by the full potential-energy hypersurface. We have already demonstrated that some of this energy is deposited into the vibrational degree of freedom. We turn our attention to the rotational degree of freedom.

Before continuing with our analysis of the rotational distributions, we must consider the possibility of rotational-state-changing collisions *subsequent* to molecular formation. As rotational-state-changing events are more probable than vibrational-state-changing events for hydrogen, the rotational distributions will be more sensitive to such events. We must consider two distinct processes that can alter the rotational distribution of nascent hydrogen molecules at the surface. These are surface-to-molecule angular momentum transfer and intramolecular rotational-to-translational (R-T) energy transfer.

Angular momentum transfer upon collision with the surface is hindered by the large rotational energy spacing of molecular hydrogen and by the $\Delta J =$ even selection rule that rotational-state-changing collisions of H_2 and D_2 must obey. Also, H_2 and D_2 are almost spherical and therefore very difficult to torque during collision. Therefore, we expect their average rotational energy to be little affected by this process. HD, however, is asymmetric; its center of mass does not lie on its geometric center, and it obeys a $\Delta J = \pm 1, \pm 2$, etc. selection rule for rotational-state-changing collisions. Thus, HD is much more likely to undergo angular momentum transfer in a molecule–surface collision than is either H_2 or D_2.[72] This effect would increase the average rotational energy of HD relative to H_2 and D_2. It appears that $\langle E_{\rm rot} \rangle (\rm HD)$ is not significantly higher than $\langle E_{\rm rot} \rangle (H_2)$ and $\langle E_{\rm rot} \rangle (D_2)$ and that $\langle E_{\rm rot} \rangle$ is much lower than the surface temperature in all cases. Were transfer of angular momentum by collision with the surface efficient, we would expect $\langle E_{\rm rot} \rangle (\rm HD)$ to be greater than the values for H_2 and D_2; thus, we conclude that surface-to-molecule angular momentum transfer is inefficient in this system.

Rotational-to-translational energy transfer causes rotational cooling in the desorption of a *chemisorbed* molecule such as NO (See Ref. 73, and references therein). In this mechanism rotational energy is transferred into translation directed away from the surface. Calculations[74] have shown that the anisotropy of the molecular potential is one of the essential elements for reproducing large amounts of rotational energy transfer.

The rotational cooling observed here is unlikely to be caused by intramolecular R-T energy transfer along the exit channel. The nearly spherical shape of H_2 and D_2 makes them unlikely to undergo R-T energy transfer. The hydrogen molecule has almost no attractive interaction with a Si surface, experiencing only an extremely weak van der Waals force at large displacements from the surface. Little energy transfer[75,76] is to be expected between the surface and a newly formed hydrogen molecule because of the weak attractive interaction and because linear momentum transfer is hindered by the large mass mismatch between molecular hydrogen and Si. HD has a much higher probability of undergoing intramolecular R-T energy transfer[72] than either H_2 or D_2 for the same reasons discussed above concerning surface-to-molecule angular momentum transfer. Therefore, were R-T energy transfer the mechanism for rotational cooling, we

would expect HD to have the lowest average rotational energy and H_2 and D_2 to show little deviation from T_s. All three isotopomers, however, are characterized by approximately the same $\langle E_{\rm rot} \rangle$, and its value is much lower than kT_s. Thus, once the molecule has formed, the energy distribution of the hydrogen molecule is unlikely to be perturbed significantly by intermolecular rotational-to-translational energy transfer.

Because we can neglect the effects of rotational-state-changing events after molecular formation, low rotational excitation demands that little torque is applied to the molecules during recombination. Thus, we focus on the characteristics of the potential-energy hypersurface that determine the observed rotational distributions. The low rotational excitation must result from some dynamical constraint on the recombination of molecular hydrogen. This constraint is unlikely to arise from the interatomic interaction potential of hydrogen. Theoretical calculations[77,78] on the three-body, gas-phase recombination of H_2 do not support the idea that molecular formation is unusually biased toward low-impact-parameter collisions. A more likely explanation is that the recombination occurs on a potential-energy hypersurface that does not resemble the gas-phase H–H interaction potential because of the presence of the Si surface. Rotational distributions colder than the surface will result if the H/Si hypersurface favors recombinative desorption from pathways that proceed through low-torque trajectories.

Gradients in the potential-energy hypersurface can lead to a torque on the recombining molecule. The convolution of molecular orientation in both z, the height of each atom above the surface, and ϕ, the azimuthal angle, with the functional dependence of the hypersurface corrugation on z and ϕ, would be the determining factor in the excitation of rotations caused by gradients.

A second process that can influence the angular momentum of desorbed hydrogen is the angular momentum associated with the collision leading to the transition state. Regardless of the mechanism of recombination, two hydrogen atoms must move toward one another to get close enough to form a bond. This collision can be characterized by the relative velocity of the hydrogen atoms toward one another, $\mathbf{v}_{\rm rel}$, and an impact parameter, $\mathbf{b}$.[79] The impact parameter is the closest center-to-center interatomic distance exclusive of the effects of the interaction potential. The angular momentum associated with this collision is proportional to the vector cross product of $\mathbf{v}_{\rm rel}$ and $\mathbf{b}$. Even if recombination occurred in a region of the hypersurface with flat energy contours, the angular momentum of the collision complex could lead to rotational excitation of the desorbed molecule. Since we have already stated, in accord with the observed vibrational populations, that the interatomic distance at the transition state is larger than the equilibrium bond distance of H_2, we would expect $\mathbf{b}$ to be large unless the H atoms are constrained to approach each other along the newly forming bond.

A velocity associated with diffusion of $H_{(a)}$ preceding recombination is necessary for the collision complex to attain significant angular momentum. Recent experiments[80] on the diffusion of $H_{(a)}$/Si(111)–(7×7) have shown that the barrier to diffusion is $E_{\rm diff} = 1.5 \pm 0.2$ eV. This value is substantially higher than that found for diffusion on metals (typically $E_{\rm diff} \approx 0.3$ eV) and represents approximately 50% of the total Si–H binding energy (vs $<20\%$ for metals). The Arrhenius prefactor, however, is found to be comparable to that for diffusion on metals. Thus, Reider Höfer, and Heinz[80] concluded that diffusion of $H_{(a)}$ on Si(111)–(7×7) proceeds through thermally activated hopping in much the same manner as on metals. The extremely large activation energy and degree of corrugation experienced by a diffusing H atom on Si distinguish this process from the diffusional process that occurs on the surfaces of metals. Whereas $H_{(a)}$ is virtually free to traverse the surface of a metal prior to desorption,[41] $H_{(a)}$ diffusion on Si(111)–(7×7) is slow but nonetheless still takes place at the desorption temperature of molecular hydrogen.

Because we have observed excess energy in the vibrational degree of freedom directly and can assume that the translational degree of freedom will also exhibit superthermal energy content,[65] we might also expect some excess energy to be deposited in the rotational degree of freedom. We observe, however, rotational distributions that are roughly one-half of the surface temperature. Specifically, the observed average rotational energies are $\langle E_{\rm rot} \rangle (v=0) = 345 \pm 83$ K, 451 ± 77 K, and 332 ± 57 K, for H_2, D_2, and HD, respectively, and $\langle E_{\rm rot} \rangle (v=1) = 348 \pm 95$ K, 385 ± 70 K, and 330 ± 54 K for H_2, HD, and D_2, respectively. These values represent significantly colder rotational distributions than observed by Kubiak, Sitz, and Zare[2] for Cu ($\langle E_{\rm rot} \rangle \approx 0.8$ to $0.9\ kT_s$). Because of the extent of the observed rotational cooling, we conclude that the recombining molecule receives little torque during recombination.

That little torque is applied to recombining hydrogen implies some combination of the following: (1) the potential-energy hypersurface is relatively flat in the region of recombination, (2) the recombining hydrogen molecule is oriented symmetrically relative to the hypersurface corrugation, and (3) little angular momentum is associated with the collision complex leading to the transition state.

A unique feature of the reconstructed Si(100)–(2×1) surface is the presence of rows of dimers (see Fig. 1). Dimer rows and first-order hydrogen desorption kinetics are also present on the Ge surface as noted above but absent on the Si(111)–(7×7) surface. One possible influence on the recombination dynamics would be the presence of dimer rows and the geometric and energetic corrugation introduced by them. The rotational degree of freedom samples this highly anisotropic electronic structure by changing the relative orientation of the molecule. Thus an analysis of the rotational distributions involves the convolution of the anisotropies of the molecule and the surface.

The model of Nørskov and co-workers[66–68] is able to reproduce the effects of the hydrogen molecule's electronic asymmetry. That is, it predicts that the lowest-energy pathway for hydrogen dissociation is that in which the molecule is parallel to the surface. This prediction is confirmed for the H/Cu system by the cluster calculations of Madhavan and Whitten.[81] That a parallel approach is the lowest-energy pathway is intuitively obvious once we have identified the

filling of the antibonding resonance as an essential element in hydrogen dissociation. Maximum overlap between the hydrogen antibonding level and the electronic structure of the surface occurs in this configuration; thus donation into the antibonding level is facilitated by the parallel approach. Therefore, we predict that a parallel approach will also be the lowest-energy pathway for hydrogen dissociation on Si and that rotation out of the plane of the surface will hinder adsorption. Hence, we concentrate on the effects of in-plane rotation.

In-plane rotational motion forces the molecule to sample the azimuthal anisotropy of the surface electronic structure. A jellium picture is unsatisfactory for the description of the Si(100)–(2×1) surface because of the localization of the dangling-bond states and the band gap. Nevertheless, guided by the insight of the Nørskov model and chemical intuition, we can predict what the effect of in-plane rotation will be.

The two potential adsorption sites that are closest geometrically are encompassed by the dangling-bond states of Si atoms on one dimer unit; cf. Figs. 1 and 5. The dangling-bond electrons also occupy the highest-energy electronic states at the surface.[13,16] The interaction of an approaching H_2 with these electronic states initiates H–H bond scission and Si–H bond formation. A hydrogen molecule that is aligned with a dimer will have the greatest overlap with the occupied and unoccupied dangling-bond states. In-plane rotation will move the molecule away from a position of maximum overlap. Thus, *the lowest-energy pathway for adsorption is an approach that is not only parallel to the surface but also aligned with the dimer.* In-plane rotation will, therefore, hinder adsorption. The implications of this adsorption mechanism are twofold.

First, detailed balance demands that the same pathway be followed in desorption. Therefore, the lowest-energy pathway for desorption is recombination across a dimer pair. This conclusion conflicts with the results of Wu and Carter, who found a large activation barrier for this pathway.[82] The desorption trajectory will likewise be parallel to the surface. This scenario will ensure a highly symmetric transition state and lead to low rotational excitation in desorption. Furthermore, since the atoms recombine by means of a more or less concerted mechanism, little angular momentum is associated with the "collision" that leads to the transition state. Therefore recombination across a dimer fulfills both of the conditions required to reproduce the low rotational excitation we observe.

Second, pairing will occur in the adsorption of *molecular* hydrogen. Boland[23] has performed STM and STS experiments on the H/Si(100)–(2×1) system that show that, even though H-*atom* adsorption proceeds randomly, diffusion induced by annealing the surface at temperatures below the desorption temperature leads to a pairing of H atoms on the dimers. The driving force for this pairing has been identified as the breaking of a π-bonding interaction between the dangling bond orbitals. No evidence for pairing was observed in the isotopic mixing experiments of Sinniah *et al.*[29] This lack of evidence may result from complications arising from the pick-off reaction they observed.

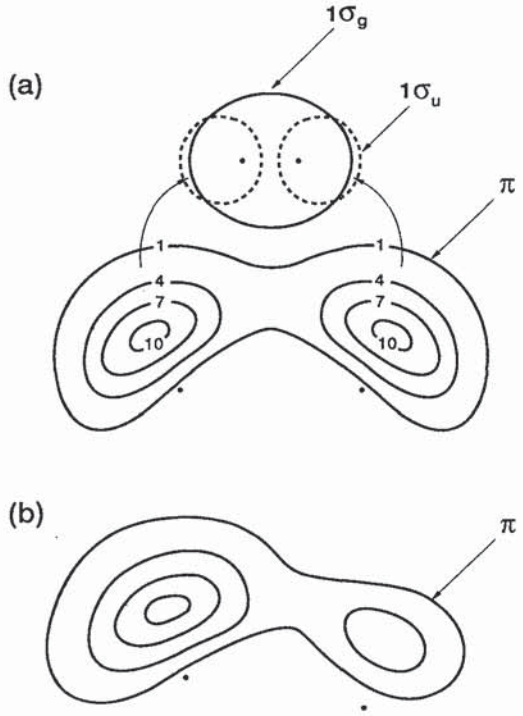

FIG. 5. Representation of the most important electronic states involved in the approach of a hydrogen molecule to a Si(100) dimer unit. The hydrogen bonding, $1\sigma_g$, and antibonding, $1\sigma_u$, orbitals are modeled after Mulliken and Ermler (Ref. 92). (a) The electron density of the symmetric Si dimer's highest-energy occupied orbital, π, modeled after the calculation of Appelbaum, Baraff, and Hamann (Ref. 13). (b) The electron density of the asymmetric Si dimer modeled after the calculation of Zhu, Nobuyuki, and Tsukada (Ref. 16).

The influence of the dangling-bond π interaction can be understood as follows. The two lone pair electrons of a dimer's dangling bonds can stabilize the clean dimer by interacting with one another. A net stabilization of 0.22–0.52 eV (Ref. 22) or 0.8 eV results.[13,23] A similar π-bonding interaction on the C(111)–diamond surface leads to a chain-like (2×1) reconstruction[83,84] and contributes to the Si(111)–(2×1) reconstruction.[85] Arguments against a pairing mechanism based on energetics[29] did not account for this π-bonding interaction.

An adsorbed H atom breaks the π-bonding interaction because one of the electrons formerly involved in the π bond partakes in the Si–H bond and the other is left unstabilized. Energetically, a second H atom is more likely to adsorb onto a lone dangling bond rather than break the π-bonding interaction of a second dimer pair. That this does not happen in H-atom adsorption is likely caused by a kinetic constraint. Even though an incident H atom may hunt for a site before adsorbing, the bonding interaction with a Si atom is so strong, roughly 3 eV, the 1 eV stabilization of the π-bonding interaction is insufficient to lead to pairing during *atomic* adsorption. Convincing evidence for the existence of pairing prior to desorption stems from first-order desorption kinetics[29] and the presence of an energetic factor, as observed in the work of Boland,[23] in addition to an orientational factor,

as postulated in our analysis of the observed rotational distributions.

We must emphasize that pairing leads to the lowest-energy final state as a result of breaking only one π bond vs breaking two π bonds should the two H atoms adsorb on two different dimers. However, Fig. 5 may be misleading in suggesting that the H_2 molecule is not only parallel and aligned with the dimer, but also that it is centered above it. The results presented here are consistent with such a four-center transition state (H_2 molecule centered above the dimer), but do not rule out a three-center transition state.

Preliminary results of H_2 desorption from Si(111) suggest the H_2 molecule is more likely to be much closer to *one* end of the dimer.[86] Evidence for a three-center transition state is discussed in more detail in Ref. 86. Here, we outline the main evidence supporting this transition-state configuration. In considering the extent of vibrational excitation we noted that the H–H internuclear separation is not too different from the equilibrium bond distance of gas-phase H_2. To interact fully with both ends of the dimer, the H_2 molecule would have to stretch significantly; cf. $r_e^{H_2} = 0.74$ Å vs $r_{\text{dimer}}^{\text{Si-Si}} = 2.4$ Å. A symmetric four-center transition state may be symmetry forbidden by the Woodward–Hoffman rules[87] should these be applicable to surface reactions. (See Ref. 88 for a discussion of the application of the Woodward–Hoffman rules to surface reactions.) Also of interest is that theoretical calculations[89–91] have found that the addition of H_2 to Si_2H_4 follows a mechanism in which H_2 inserts into one end of H_2Si–SiH_2 to form a H_4Si–SiH_2 complex followed by a rapid migration of one H atom to form H_3Si–SiH_3.

We propose the following mechanism of hydrogen desorption from Si(100)–(2×1). The desorption process starts from a paired set of hydrogen atoms on one dimer unit. One of the hydrogen atoms migrates to the other side of the dimer to initiate a concerted desorption mechanism that passes through a symmetric three-center transition state. The possibility of a concerted elimination type of desorption mechanism has also been raised by Nachtigall, Jordan, and Janda.[22]

The trajectory described here represents a highly constrained geometry in the transition state. A transition-state theory analysis of the desorption rate expression[40] demands that a constrained geometry leads to a low value of the Arrhenius prefactor. The value reported by Sinniah *et al.* is rather low and suggests a highly constrained transition-state geometry. Neither the value of A nor our internal-state distributions appears to support the band-state model of Sinniah *et al.* We believe pairing occurs prior to desorption, and desorption proceeds through a concerted mechanism with a symmetric transition state. Further theoretical and experimental studies are required, however, to determine the geometry of and the pathway to the transition state.

V. CONCLUSION

We have obtained vibrational- and rotational-state distributions for H_2, HD, and D_2, thermally desorbed from Si(100)–(2×1) surfaces. The observation of superthermal population in the $v = 1$ state suggests that the transition state leading to desorption is characterized by an elongated H–H distance as compared with the gas-phase equilibrium bond distance of H_2. Observation of the same relative vibrational enhancement factor for all three isotopomers indicates that tunneling is not important in the population of the $v = 1$ level within our error bars. The average rotational energies (expressed in temperature units) are significantly lower than the surface temperature and exhibit no isotopic dependence. The data presented here, coupled with the known dynamics of recombinative desorption and the electronic structure of Si(100)–(2×1), lead to the conclusion that pairing of adsorbed H on Si dimer atoms occurs prior to desorption and that such pairing will be observed in the adsorption of molecular hydrogen. Furthermore, we propose that the desorption trajectory passes through a symmetric three-center transition state. These results suggest that not only the energy of the incident molecule but also its orientation, in terms of both the rotational axis and the lattice impact parameter during collision with the surface, are important variables in determining the sticking coefficient of H_2 onto Si(100)–(2×1).

ACKNOWLEDGMENTS

Funding was provided by the Office of Naval Research under Grant No. N00014-91-J1023. K. W. K. acknowledges the Proctor & Gamble Foundation and Phi Beta Kappa of Northern California for fellowships. S. F. S. acknowledges support from a National Science Foundation Graduate Fellowship. We also thank J. Boland, W. Ho, and K. Janda for relaying experimental results prior to publication.

[1] M. C. Lin and G. Ertl, Annu. Rev. Phys. Chem. **37**, 587 (1986).
[2] G. D. Kubiak, G. O. Sitz, and R. N. Zare, J. Chem. Phys. **83**, 2538 (1985).
[3] R. P. Thorman and S. L. Bernasek, J. Chem. Phys. **74**, 6498 (1981).
[4] L. Schröter, H. Zacharias, and R. David, Phys. Rev. Lett. **62**, 571 (1989).
[5] X. R. Chen, K. Wagemann, J. Wanner, W. Brenig, and S. Küchenhoff, Surf. Sci. **224**, 570 (1989).
[6] H. Zacharias, J. Mod. Phys. B **4**, 45 (1990).
[7] D. Haneman, Rep. Prog. Phys. **50**, 1045 (1987).
[8] J. A. Schaefer, Physica B **170**, 45 (1991).
[9] R. M. Tromp, R. J. Hamers, and J. E. Demuth, Phys. Rev. Lett. **55**, 303 (1985).
[10] R. J. Hamers, R. M. Tromp, and J. E. Demuth, Phys. Rev. B **34**, 5343 (1986).
[11] R. M. Tromp, R. J. Hamers, and J. E. Demuth, Science **234**, 304 (1986).
[12] R. J. Hamers, P. Avouris, and F. Bozso, Phys. Rev. Lett. **59**, 2071 (1987).
[13] J. A. Appelbaum, G. A. Baraff, and D. R. Hamann, Phys. Rev. B **14**, 588 (1976).
[14] A. Redondo and W. A. Goddard III, J. Vac. Sci. Technol. **21**, 344 (1982).
[15] J. Pollmann, P. Kruger, and A. Mazur, J. Vac. Sci. Technol. B **5**, 945 (1987).
[16] Z. Zhu, S. Nobuyuki, and M. Tsukada, Phys. Rev. B **40**, 11 868 (1989).
[17] B. I. Craig and P. V. Smith, Surf. Sci. **218**, 569 (1989).
[18] B. I. Craig and P. V. Smith, Surf. Sci. **226**, L55 (1990).
[19] E. Artacho and F. Ynduráin, Phys. Rev. Lett. **62**, 2491 (1989).
[20] G. P. Kochanski and J. E. Griffith, Surf. Sci. **249**, L293 (1991).
[21] D. J. Chadi, Phys. Rev. Lett. **43**, 43 (1979).
[22] P. Nachtigall, K. D. Jordan, and K. C. Janda, J. Chem. Phys. **95**, 8652 (1991).
[23] J. J. Boland, Phys. Rev. Lett. **67**, 1539 (1991).
[24] G. Schulze and M. Henzler, Surf. Sci. **124**, 336 (1983).
[25] H. Froitzheim, U. Köhler, and H. Lammering, Surf. Sci. **149**, 537 (1985).
[26] B. G. Koehler, C. H. Mak, D. A. Arthur, P. A. Coon, and S. M. George, J. Chem. Phys. **89**, 1709 (1988).

[27] M. L. Wise, B. G. Koehler, P. Gupta, P. A. Coon, and S. M. George, Surf. Sci. **258**, 166 (1991).
[28] U. Jansson and K. Uram, J. Chem. Phys. **91**, 7978 (1989).
[29] K. Sinniah, M. G. Sherman, L. B. Lewis, W. H. Weinberg, J. T. Yates, Jr., and K. C. Janda, J. Chem. Phys. **92**, 5700 (1990).
[30] B. I. Craig and P. V. Smith, Physica B **170**, 518 (1991).
[31] S. Ciraci, R. Butz, E. M. Oellig, and H. Wagner, Phys. Rev. B **30**, 711 (1984).
[32] J. T. Law, J. Phys. Chem. **30**, 1568 (1959).
[33] Y. I. Belyakov, N. I. Ionov, and T. N. Kompaniets, Fiz. Tverd. Tela (Leningrad) **14**, 2992 (1972) [Sov. Phys. Solid State **14**, 2567 (1973)].
[34] M. I. Datsiev and Y. I. Belyakov, Zh. Tekh. Fiz. **40**, 229 (1970) [Sov. Phys. Tech. Phys. **15**, 166 (1970)].
[35] H. Ibach and J. E. Rowe, Surf. Sci. **43**, 481 (1974).
[36] G. A. Reider, U. Höfer, and T. F. Heinz, J. Chem. Phys. **94**, 4080 (1991).
[37] A. V. Hamza, G. D. Kubiak, and R. H. Stulen, Surf. Sci. **237**, 35 (1990).
[38] J. E. Crowell (private communication).
[39] D. A. Outka, Surf. Sci. **235**, L311 (1990).
[40] V. P. Zhdanov, Surf. Sci. Rep. **12**, 183 (1991).
[41] K. Christmann, Surf. Sci. Rep. **9**, 1 (1988).
[42] K. J. Uram and U. Jansson, J. Vac. Sci. Technol. B **7**, 1176 (1989).
[43] F. Bozso and P. Avouris, Phys. Rev. B **38**, 3943 (1989).
[44] K. J. Uram and U. Jansson, Surf. Sci. **249**, 105 (1991).
[45] Y. Suda, D. Lubben, T. Motooka, and J. E. Greene, J. Vac. Sci. Technol. B **7**, 1171 (1989).
[46] J. J. Boland, Phys. Rev. B **44**, 1383 (1991).
[47] S. F. Shane, K. W. Kolasinski, and R. N. Zare, J. Vac. Sci. Technol. A (in press).
[48] K.-D. Rinnen, M. A. Buntine, D. A. V. Kliner, R. N. Zare, and W. M. Huo, J. Chem. Phys. **95**, 214 (1991).
[49] The β-bariuim borate crystal was supplied by R. S. Feigelson and R. K. Route and grown as part of a research program sponsored in part by the Army Research Office, Contract No. DAAL03-86-K-0129, and in part by the NSF/MRL Program through the Center for Materials Research, Stanford University.
[50] S. M. Gates, Surf. Sci. **195**, 307 (1988).
[51] S. M. Gates, C. M. Greenlief, D. B. Beach, and R. R. Kunz, Chem. Phys. Lett. **154**, 505 (1989).
[52] R. Butz, R. Memeo, and H. Wagner, Phys. Rev. B **25**, 4327 (1982).
[53] J. Misewich, P. L. Houston, and R. P. Merrill, J. Chem. Phys. **82**, 1577 (1985).
[54] J. Misewich, H. Zacharias, and M. M. T. Loy, Phys. Rev. Lett. **55**, 1919 (1985).
[55] J. Misewich, C. N. Plum, G. Blyholder, R. L. Houston, and R. P. Merrill, J. Chem. Phys. **78**, 4245 (1983).
[56] L. Schröter, H. Zacharias, and R. David, Appl. Phys. A **41**, 95 (1986).
[57] J. Harris, T. Rahman, and K. Yang, Surf. Sci. **198**, L312 (1988).
[58] J. C. Polanyi, Acc. Chem. Res. **5**, 161 (1972).
[59] J. H. McCreery and G. Wolken, Jr., J. Chem. Phys. **67**, 2551 (1971).
[60] D. Halstead and S. Holloway, J. Chem. Phys. **93**, 2859 (1990).
[61] S. Küchenhoff, W. Brenig, and Y. Chiba, Surf. Sci. **245**, 389 (1991).
[62] B. E. Hayden and C. L. A. Lamont, Surf. Sci. **243**, 31 (1991).
[63] K. D. Rendulic, G. Anger, and A. Winkler, Surf. Sci. **208**, 404 (1989).
[64] H. A. Michelsen and D. J. Auerbach, J. Chem. Phys. **94**, 7502 (1991).
[65] W. Ho (private communication).
[66] B. I. Lundqvist, J. K. Nørskov, and H. Hjelmberg, Surf. Sci. **80**, 441 (1979).
[67] J. K. Nørskov, S. Holloway, and N. D. Lang, Surf. Sci. **137**, 65 (1984).
[68] P. K. Johansson, Surf. Sci. **104**, 510 (1981).
[69] J. Harris, Appl. Phys. A **47**, 63 (1988).
[70] J. Harris and S. Andersson, Phys. Rev. Lett. **55**, 1583 (1985).
[71] W. Mönch, P. Koke, and S. Krueger, J. Vac. Sci. Technol. **19**, 313 (1981).
[72] J. P. Cowin, C.-F. Yu, S. J. Sibener, and L. Wharton, J. Chem. Phys. **79**, 3537 (1983).
[73] D. C. Jacobs, K. W. Kolasinski, S. F. Shane, and R. N. Zare, J. Chem. Phys. **91**, 3182 (1989).
[74] C. W. Muhlhausen, L. R. Williams, and J. C. Tully, J. Chem. Phys. **83**, 2594 (1985).
[75] B. M. Rice, I. NoorBatcha, D. L. Thompson, and L. M. Raff, J. Chem. Phys. **86**, 1608 (1987).
[76] L. M. Raff, I. NoorBatcha, and D. L. Thompson, J. Chem. Phys. **85**, 3081 (1986).
[77] N. C. Blais and D. G. Truhlar, J. Chem. Phys. **66**, 772 (1977).
[78] N. C. Blais and D. G. Truhlar, J. Chem. Phys. **74**, 6709 (1981).
[79] R. D. Levine and R. B. Bernstein, *Molecular Reaction Dynamics and Chemical Reactivity* (Oxford University, New York, 1987).
[80] G. A. Reider, U. Höfer, and T. F. Heinz, Phys. Rev. Lett. **66**, 1994 (1991).
[81] P. Madhavan and J. L. Whitten, J. Chem. Phys. **77**, 2673 (1982).
[82] C. J. Wu and E. A. Carter, Chem. Phys. Lett. **185**, 172 (1991).
[83] G. D. Kubiak and K. W. Kolasinski, Phys. Rev. B **39**, 1381 (1989).
[84] E. C. Sowa, G. D. Kubiak, R. H. Stuhlen, and M. A. Van Hove, J. Vac. Sci. Technol. A **6**, 832 (1988).
[85] K. C. Pandey, Phys. Rev. Lett. **47**, 1913 (1981).
[86] S. F. Shane, K. W. Kolasinski, and R. N. Zare (unpublished).
[87] R. B. Woodward and R. Hoffmann, *The Conservation of Orbital Symmetry* (Verlag Chemie, Weinheim, 1969).
[88] R. I. Masel, Catal. Rev. Sci. Eng. **28**, 335 (1986).
[89] M. S. Gordon, T. N. Truong, and E. K. Bonderson, J. Am. Chem. Soc. **108**, 1421 (1986).
[90] P. Ho, M. E. Coltrin, J. S. Binkley, and C. F. Melius, J. Phys. Chem. **90**, 3399 (1986).
[91] P. M. Agrawal, D. L. Thompson, and L. M. Raff, J. Chem. Phys. **92**, 1069 (1990).
[92] R. S. Mulliken and W. C. Ermler, *Diatomic Molecules: Results of Ab Initio Calculations* (Academic, New York, 1977).